Applied Energy 162 (2016) 330–345

Contents lists available at ScienceDirect

Applied Energy

journal homepage: www.elsevier.com/locate/apenergy

Optimum design of horizontal ground-coupled heat pump systems using spiral-coil-loop heat exchangers

Gyu-Hyun Go, Seung-Rae Lee *, Seok Yoon, Min-Jun Kim

Department of Civil and Environmental Engineering, KAIST, Daejeon 305-701, Republic of Korea

HIGHLIGHTS

- Optimum design of horizontal ground heat pump systems is presented.
- Accuracy of numerical model is verified through indoor thermal response tests.
- A total of 160 parametric studies are conducted using numerical simulation models.
- Heat efficiencies are compared for 160 major combinations of design factors.
- Optimum design conditions are suggested using several economic analysis tools.

ARTICLE INFO

Article history:
Received 27 May 2015
Received in revised form 14 October 2015
Accepted 17 October 2015

Keywords:
Horizontal ground heat exchanger
Thermal response test
Numerical simulation
Parametric studies
Optimum design

ABSTRACT

This paper deals with an optimum design of horizontal ground heat pump systems for spiral-coil-loop heat exchangers. A three dimensional numerical analysis model simulating the thermal behavior of a horizontal spiral-coil-loop heat exchanger was developed, and the accuracy of the model was verified through indoor thermal response tests. After that, a total of 160 parametric studies were conducted using numerical simulation models in order to grasp the degree of effects that key input parameters used in the model would have on the output. Then, an optimum design condition for horizontal ground coupled heat pump system was suggested using several economic analysis tools. Economic analysis factors, such as internal rate of return, savings to investment ratio, and simple payback period, show that certain design conditions (coil pitch: 0.08 m, setting depth: 2.5 m, circulating fluid velocity: 0.7 m s^{-1}) provide the most economic feasibility. However, this condition also varies with the unit cost of operation and initial investment.

1. Introduction

Due to the recent rise in fuel costs and global warming problems, interest in alternative energy sources that are renewable and pollute less, has gradually increased. Particularly, ground-coupled heat pump systems (GCHPs) have been recognized to be highly cost effective and environmentally friendly for space heating and cooling of buildings [1–5]. This system uses relatively constant ground temperatures as a heat reservoir: heat source for heating in winter, and heat sink for cooling in summer. The GCHPs are classified into open and closed loop systems; the most common system is a vertical closed system with deep borehole ground heat exchangers (GHEs). However, high initial installation costs related to the drilling operation have been considered a fatal drawback of vertical borehole GHEs. Thus, horizontal ground-coupled heat pump systems (HGCHPs) are often preferred over vertical systems if the site has adequate space. Owing to the lower initial installation costs, the use of horizontal ground heat exchangers (HGHEs) can provide a viable alternative solution that reaches a good compromise between efficiency and costs [6].

The major heat transfer mechanisms of HGCHPs involve multiple processes: heat convection between the circulating fluid and the pipe, and heat conduction inside the ground. Since the HGHEs are generally buried at shallow depths (1–3 m), the heat conduction is also influenced by the land surface temperature. Thus, there have been extensive studies on the heat transfer mechanisms of HGHEs considering various ground conditions, both in the area of numerical modeling and in field experiments. For example, Tarnawski et al. [7] conducted numerical simulations of a HGCHPs operating in heating and cooling modes for a typical residential house, located in Sapporo (Japan). The selected GCHPs showed an

* Corresponding author. Tel.: +82 42 350 3617; fax: +82 42 350 7200.
E-mail address: srlee@kaist.ac.kr (S.-R. Lee).

http://dx.doi.org/10.1016/j.apenergy.2015.10.113
0306-2619/

Nomenclature

Symbol

a	half difference between the maximum and minimum annual temperatures (K)
A_p	pipe cross section area (m^2)
C_p	specific heat capacity ($J\ kg^{-1}\ K^{-1}$)
D_T	thermal diffusivity of soil ($m^2\ s^{-1}$)
f_D	coefficient of friction
hZ	equivalent convective heat transfer coefficient
h_{int}	film heat transfer coefficients inside the tube ($W\ m^{-2}\ K^{-1}$)
h_{ext}	film heat transfer coefficients outside the tube ($W\ m^{-2}\ K^{-1}$)
Q	general heat sources ($W\ m^{-3}$)
r_n	outer radius of wall n (m)
T	temperature (K)
T_{ext}	external temperature outside the pipe (K)
T_f	fluid temperature (K)
T_{in}	inlet fluid temperature (K)
T_{out}	outlet fluid temperature (K)
T_M	mean temperature in the year of the climatic zone (K)
t	time (s)
t_M	time when the maximum temperature on the ground surface occurs (day)
u	fluid velocity ($m\ s^{-1}$)

Greek letters

ρ	density ($kg\ m^{-3}$)
ρ_f	fluid density ($kg\ m^{-3}$)
ρC	equivalent volumetric heat capacity ($J\ K^{-1}\ m^{-3}$)
λ_{eff}	effective thermal conductivity of medium ($W\ m^{-1}\ K^{-1}$)
λ_f	fluid thermal conductivity ($W\ m^{-1}\ K^{-1}$)
λ_n	thermal conductivity of wall n (W/m K)
λ_{solid}	thermal conductivity of solid particle (W/m K)
λ_{pore}	thermal conductivity of pore (W/m K)
χ_{solid}	volumetric fraction
τ	period (year)

Subscripts

NPV	net present value
IRR	internal rate of return
SIR	savings to investment ratio
SPP	simple payback period (year)

overall annual COP of 3.26 and required 19.7 GJ/year of total electrical consumption, which means that 100 Yen is equivalent to about 19 kW h of heat output. For the same cost, the corresponding heat output produced by an oil furnace was around 12.5 kW h. Based on these results, the conclusion was that GCHPs is more beneficial alternatives for space heating than are oil furnaces for given geological and weather conditions. Wu et al. [8] conducted 3D numerical analyses for a slinky HGHE, and its performance was compared with that of a straight GHE. After running the systems for 140 h, the specific heat extraction of the straight pipe was 3.5 W/m higher than that of the slinky pipe. However, the heat extraction per unit length of soil for the slinky heat exchanger was significantly higher than that of the straight system. Furthermore, Sanaye and Niroomand [9] presented a thermal-economic optimal design method to obtain the various optimum design parameters of straight HGHEs. The optimum design parameters of the system were estimated by minimizing a defined objective function (total annual cost, TAC). The results show that the TAC values approximately change linearly with capacity, and that soils with greater heat transfer coefficient have lower optimized TAC. Li et al. [10] examined the groundwater effect on the performance of coil-type HGHEs, which enabled the establishment of a moving ring source model, and they analytically solved the temperature response of coil-type HGHEs using groundwater flows. According to their analysis, for the same heat extraction rate, the layout of the heat exchanger arranged perpendicular to the trench and the water flow direction exhibited the highest average tube surface temperature. Furthermore, under the same heat flux, the tube surface could recover to reach its initial level more quickly in the presence of water flow. Congedo et al. [6] conducted simulations on several different types of HGHEs using the CFD (computational fluid dynamics) code Fluent. The system performance was evaluated by considering different soil thermal conductivities, GHE configurations, heat-transfer-fluid velocities, and the depth of installation. According to their analysis, the most important parameter for the system performance was the ground thermal conductivity, and comparing the geometry arrangements led to a choice of the helical heat exchanger as the best performing one. Gonzalez et al. [11] focused on the interactions between the trench, HGHEs, and the aboveground environment; then analyzed the key factors that influence the efficiency of a HGCHPs. Their results showed that the soil temperatures and soil moisture content could change the heat transport in the soil and hence they could affect the GCHP performance. The slinky HGHE influenced soil temperatures up to 0.9 m from the installation depth in winter, and the consistent differences in soil moisture content measurements between the reference and GCHP profile could be explained by temperature-gradient-induced moisture gradients and a decrease in hydraulic conductivity due to decreased temperatures (causing increased viscosity). Fujii et al. [12] conducted long-term cooling and heating tests to compare the heat exchange capacities of double-layer slinky-coil HGHEs with single-layer HGHEs, and then they developed a numerical simulation model considering the surface boundary conditions. Through the sensitivity analyses, they suggested an optimum design depth for the double-layer HGHEs (1.5 m upper layer when the lower layer was fixed at 2.0 m). Ghong et al. [13] also evaluated the thermal performance of HGHEs using numerical analyses, and examined the effect of loop pitch, loop diameter, soil properties, and intermittent operation on system performance. According to their analysis, reducing the loop pitch/spacing of the slinky exchanger improved the overall thermal performance of the system. Moreover, the influence of loop diameter was smaller than the effect of loop pitch, and the increase of thermal diffusivity increased the overall system performance. Furthermore, running the system in intermittent operation had a higher heat transfer rate than under continuous operation. Bazkiaei et al. [14] developed a numerical model for HGCHPs with a non-homogeneous soil layer and confirmed that a non-homogeneous soil profile exhibited a great potential for enhancing a HGCHPs performance by increasing the energy extraction from the ground. Moreover, using the numerical model coupled with a generic algorithm, they suggested the operational parameters that maximize heat efficiency. The optimized seasonal energy extraction rates from the ground exhibited significant difference (an

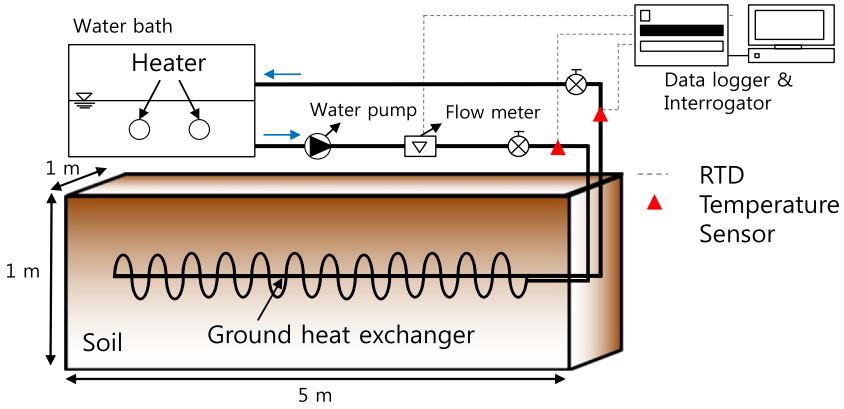

(a)

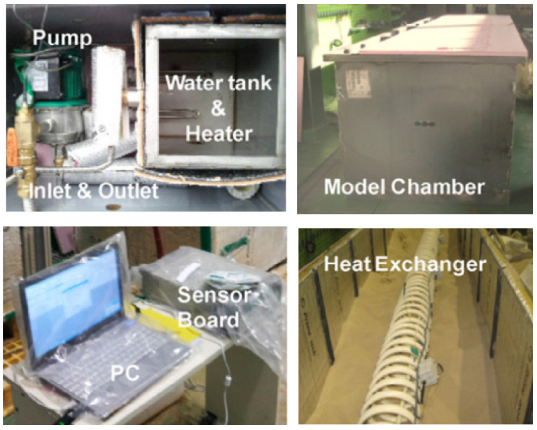

(b)

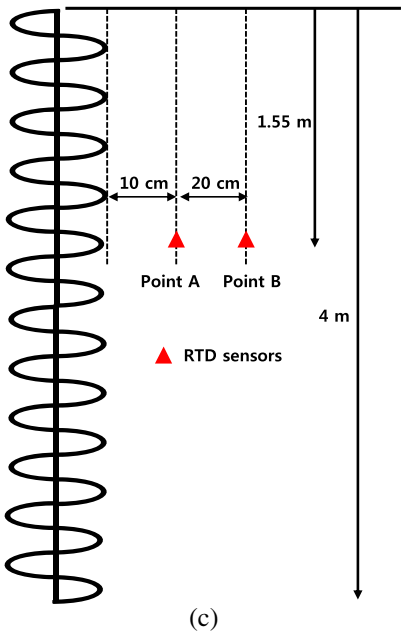

(c)

Fig. 1. Experimental system of thermal response tests: (a) Schematic diagram of thermal response tests, (b) experimental system components, (c) locations of sensors for soil temperature measurement.

upper range of 40–60% less) from the highest achievable monthly values in the heating season. Recently, Go et al. [15] suggested a new performance evaluation algorithm for HGCHPs that considers rainfall infiltration. They examined the effect of rainfall on the thermal properties of a trench; then evaluated the system performance. According to the performance test results in unsaturated ground with varying thermal conductivity profile, the rainfall infiltration increased the thermal efficiency compared with that without rainfall. The higher heat efficiency found in the rainfall period might result from the increase of the thermal conductivity in the

Table 1
Thermal properties of Joomonjin sand.

Parameters	Values
Unit dry density, γ (kN m^{-3})	1397
Thermal conductivity, λ (W m^{-1} K^{-1})	0.28
Specific heat capacity, c (J kg^{-1} K^{-1})	800
Thermal diffusivity, α (m^2 s^{-1})	2.57×10^{-7}

Table 2
Specifications of indoor thermal response tests.

Test	Coil pitch (m)	$\dot{m}$[a] (kg s^{-1})	$T_{f,in} - T_{f,out}$ (K)	Q[b] (W)
I	0.10	0.113	0.904	430
II	0.15	0.105	0.872	385
III	0.20	0.100	0.892	374
IV	0.25	0.083	0.845	296

[a] Average values obtained during test.
[b] Can be obtained by $Q = \dot{m} \cdot c\,(T_{f,in} - T_{f,out})$.

ground. This result implies that the rainfall infiltration might influence the design length of HGHEs. More recently, Adamovsky et al. [16] monitored the temperature of soil massif and analyzed heat energy transferred from the soil massif for linear HGHEs and slinky HGHEs. Both exchangers were compared in terms of their influence on the soil massif temperature in the exchanger area, and on the exchanger power output. According to their study results, the linear heat exchanger seemed to be more suitable as a low-potential power supply for heat pumps, and the average temperatures of the soil massif in the exchanger areas were positive in both heating periods and the temperature was higher with the linear exchanger. Also, Kupiec et al. [17] presented a new mathematical model for a HGHE based on the one-dimensional transient heat conduction equation with an internal source of heat. They conducted an experimental verification and confirmed that the applied model correctly describes the heat transfer in HGHEs. The model calculations also showed that a cyclic steady state is reached in the ground after about 10 years of operation under the typical

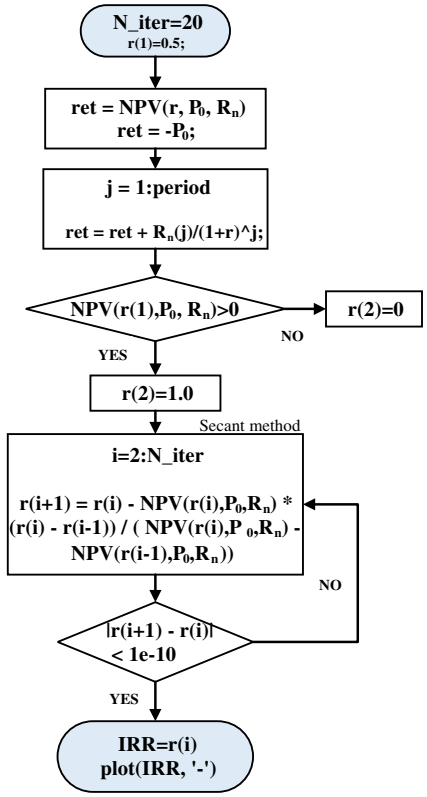

Fig. 3. Flowchart of IRR calculation algorithm using the secant method.

operating conditions of a HGHE. Furthermore, Naylor et al. [18] examined the spatiotemporal variability of ground thermal properties in glacial sediments and its implications for HGHE design. Their research suggests that expanding the characterization of soil thermal properties in specific settings where HGHPs are targeted will improve understanding of the dynamic aspects of ground heat exchange and lead to more optimal HGHP system designs.

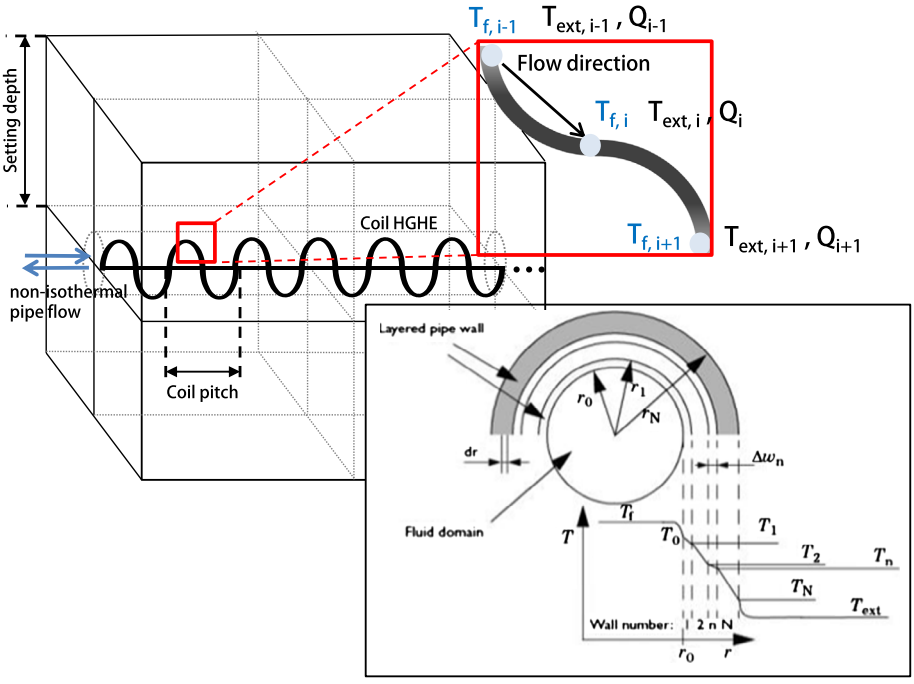

Fig. 2. Coupled process between the convective and conductive heat transfers at the heat exchanger wall.

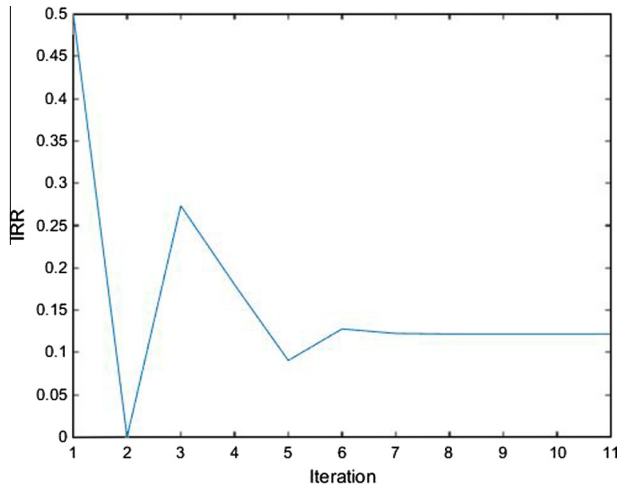

Fig. 4. IRR value calculated from the proposed algorithm.

However, although many previous studies have dealt with evaluation of system performance (energy or exergy analysis) and influencing factor analysis, little attention has been paid to the optimum design of HGCHPs, particularly for a spiral coil heat exchanger considering economic analysis tools. In addition, there are few studies that consider the environmental impacts (or benefits) of HGCHPs. Thus, this study developed a three dimensional (3D) numerical analysis model that can simulate the thermal behavior of a spiral coil HGHE (scHGHE), and then the accuracy of the model was verified using indoor thermal response tests (TRTs). After that, 160 parametric studies were conducted using numerical simulation models in order to grasp the degree of effects that key input parameters used in the model, would have on the output. From this, an optimum design for horizontal GCHPs was proposed using several economic analysis tools that could consider the economic benefits of each particular design condition. Furthermore, in order to consider the system's environmental impacts, we indicated the reduction amount of CO_2 emission of HGCHPs for each design condition compared to a typical HVAC system; then the impact of carbon credits earned on the factors in the economic analysis was analyzed.

2. Experimental setup

The thermal response tests (TRTs) of the scHGHE were conducted in a model chamber. A schematic diagram of the thermal response test set-up is shown in Fig. 1. The setup consisted of a mockup steel box, a heater, a pump, a flow meter, a water tank, and RTD (Resistance Temperature Detector) temperature sensors (Fig. 1a and b). The size of the steel box, in which soil can be compacted to a certain density, and GHEs are installed, is 5 m × 1 m × 1 m (L × W × H). A flow meter maintains a constant flow rate in the TRT system. RTD sensors were installed to measure the soil temperature and fluid temperature at inlet and outlet. The radial and axial locations of the RTD sensors (Point A and Point B) are indicated in Fig. 1(c).

The model chamber was filled with a typical Korean sand (Joomoonjin) in a dry condition. Based on the sand-raining method,

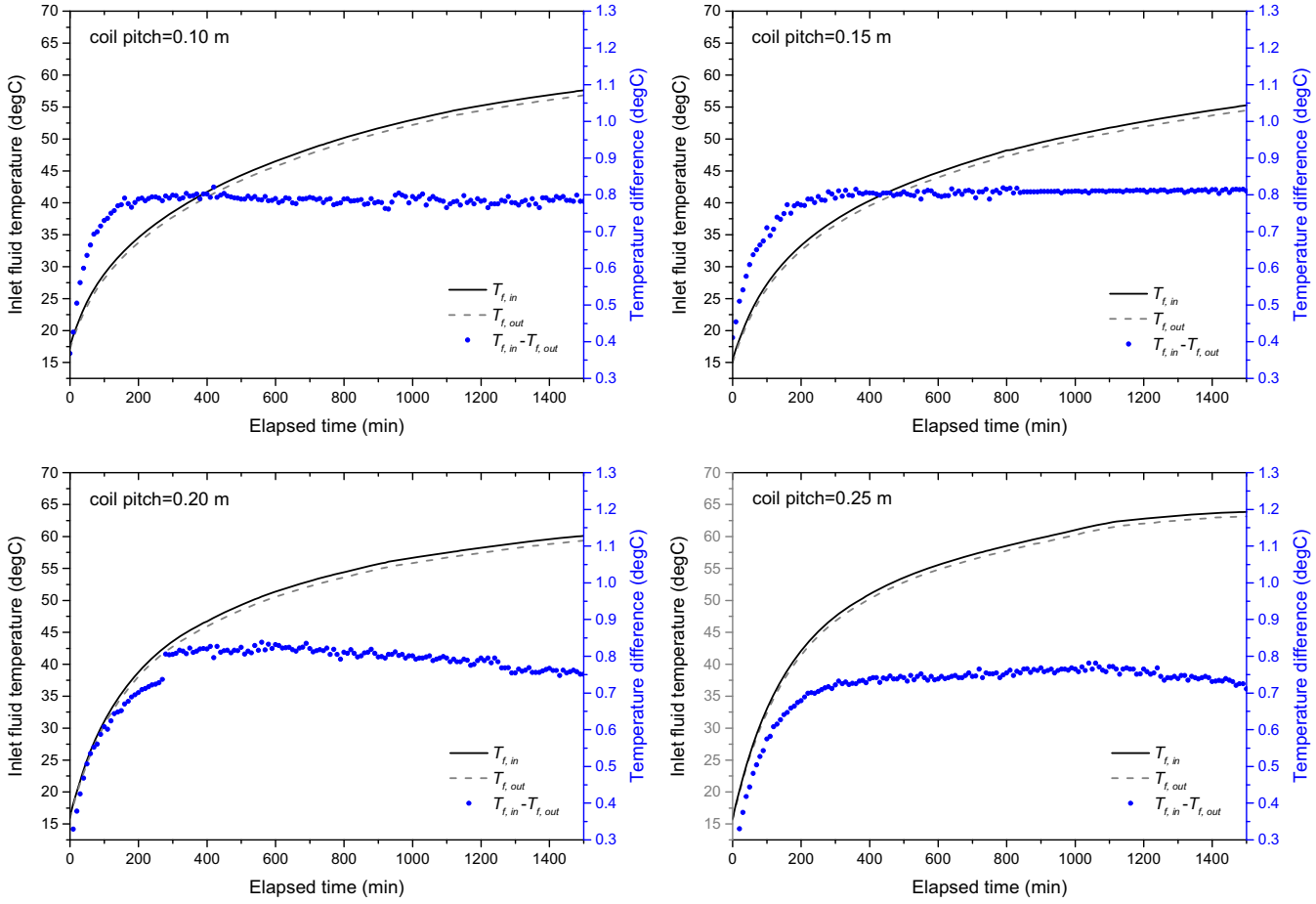

Fig. 5. Results of thermal response tests for differences in coil pitch.

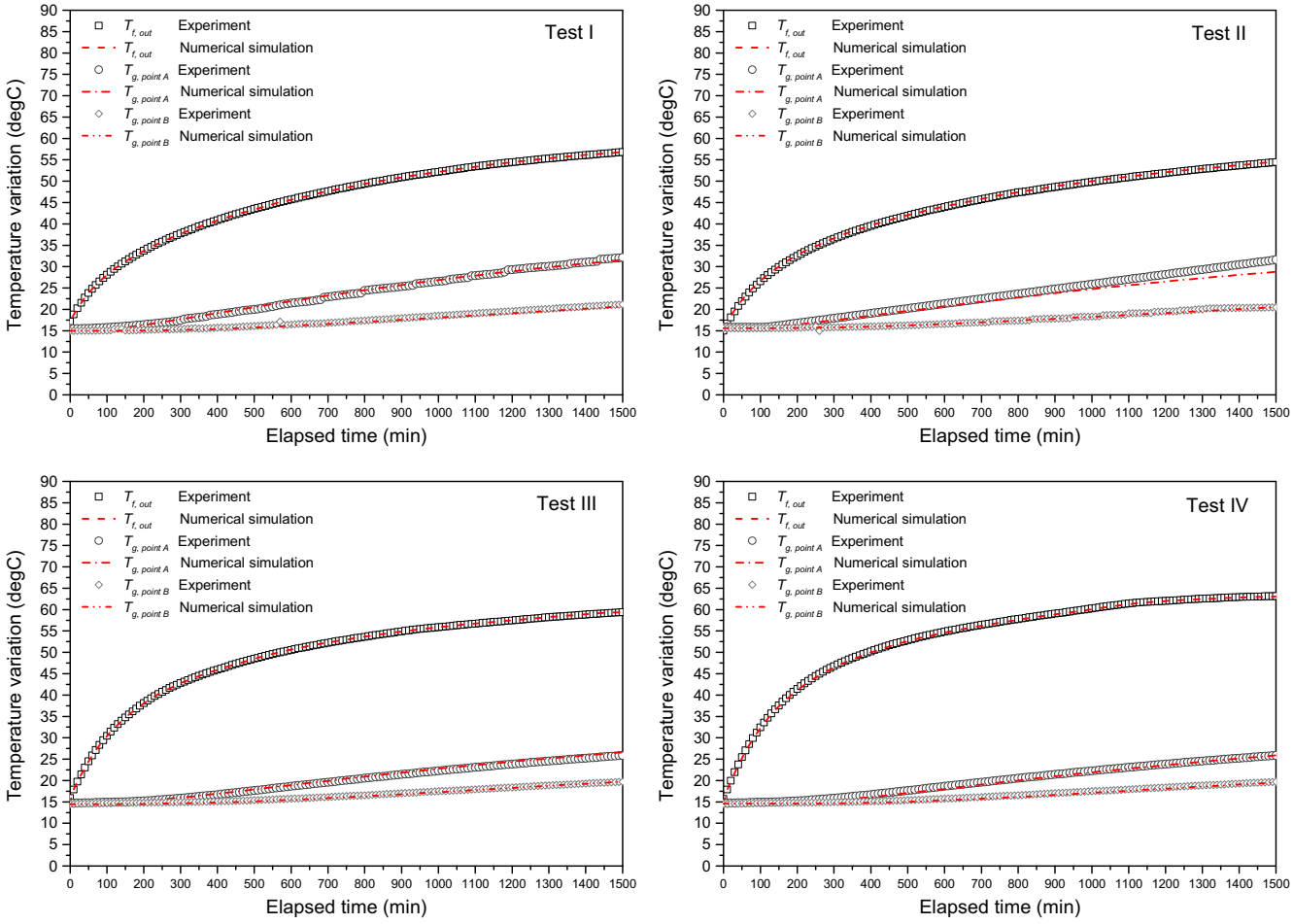

Fig. 6. Verification of three dimensional numerical simulation model via experiments.

nearly homogeneous sand was prepared in the chamber. Table 1 presents the thermal properties of the sand. The thermal conductivity of the sand given in Table 1 is the mean value of the measurements made by the steady-state heat flow meter [19] and transient needle probe method [20], which were conducted for the same unit density presented in Table 1.

For the tests, polybutylene spiral-coil heat exchangers were manufactured, of which diameter, outer pipe diameter, and thickness were 0.25 m, 0.025 m, and 0.002, respectively. The length of the axial return pipe was 4.0 m. Before conducting the TRT, flushing and purging was done to remove air bubbles and impurities from inside the pipes. As presented in Table 2, four thermal-response tests involving different coil pitches and flow rates (Test I–Test IV) were conducted during 1500 min, and the temperature variations were checked at every 10 min. The heat flux (Q) injected to the soil was calculated by the measured flow rate ($\dot{m}$) and fluid temperature difference between inlet and outlet ($T_{in} - T_{out}$).

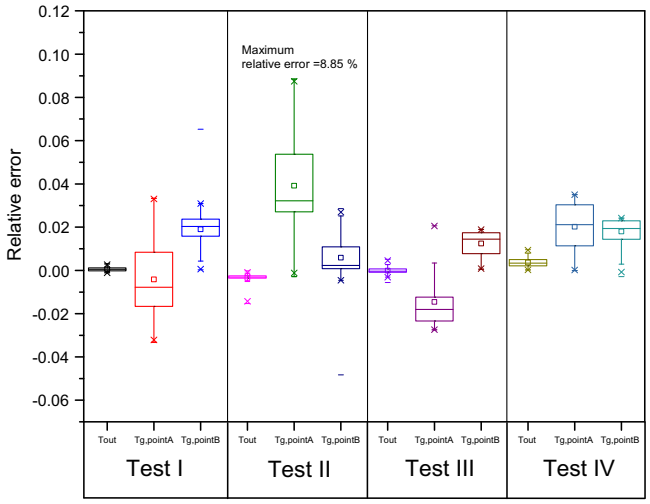

Fig. 7. Results of error analysis of the measurement.

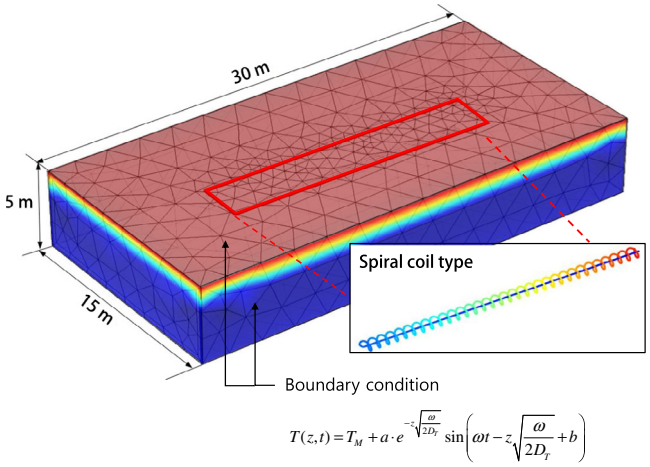

Fig. 8. Finite element model for the parametric study of horizontal ground heat exchangers.

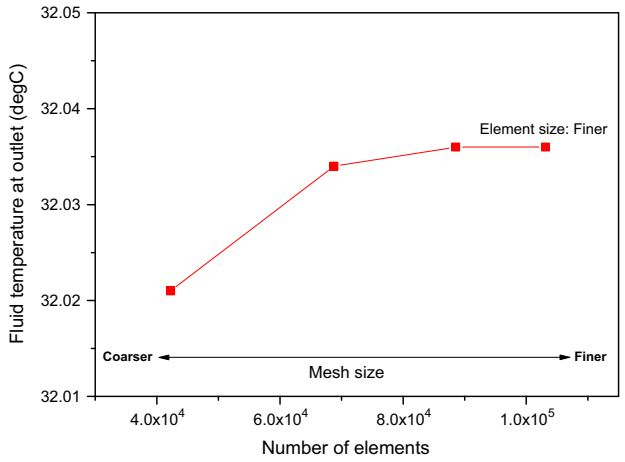

Fig. 9. Results of the grid independent tests.

Table 3
Basic thermal properties of the materials used in the numerical analysis model.

Material	Thermal conductivity ($W\,m^{-1}\,K^{-1}$)	Specific heat capacity ($J\,kg^{-1}\,K^{-1}$)	Density ($kg\,m^{-3}$)
Soil	3.00[a]	1160	1800
Polybutylene pipe[b]	0.39	525	955
Circulating water	0.60	4200	1000

[a] Equivalent thermal conductivity.
[b] Provided by the manufacturer.

Table 4
Values of the constant used in Eq. (8).

Constant	Value
T_M	15.2 °C
a	17.8 °C
τ	365 (1 year)
t_M	218 day

3. Numerical analysis

In this study, a numerical analysis model was developed to evaluate the thermal behavior of scHGHEs. The numerical analysis was performed with the commercial program COMSOL Multiphysics 5.0a [21], which is a computer code based on the finite element method (FEM), coupled with computational fluid dynamics (CFD) analysis. The newly developed numerical simulation model solves 3D heat transfer problems and ultimately calculates the thermal energy of the HGHEs. The major heat transfer mechanisms of this model involve multiple processes including heat convection between the circulating fluid and the pipe, and the heat conduction in the ground. The domain is regarded as a porous medium that can be defined by the two phases of soils (solid particles and pores). Thus, the governing equation of heat transfer in the domain, based on Fourier's law, can be expressed as follows [22]:

$$(\rho C)u\cdot\nabla T-\nabla\cdot(\lambda_{eff}\nabla T)=Q \tag{1}$$

$$\lambda_{eff}=\chi_{soild}\lambda_{solid}+(1-\chi_{solid})\lambda_{pore} \tag{2}$$

where Q indicates the general heat sources ($W\,m^{-3}$), T is the temperature of the porous medium (K) in which the local thermal equilibrium is assumed [23], and u is the fluid velocity that flows through the soils ($m\,s^{-1}$). Furthermore, λ_{eff} is the effective thermal conductivity of the medium ($W\,m^{-1}\,K^{-1}$), which can be calculated by several typical mixing models [24]. In this study, a weighted arithmetic mean model (Eq. (2)) was used, and χ_{solid} was assumed to be 0.6.

Meanwhile, the energy equation for fluid flow in a pipe can be written as in Eq. (3) [25,26]:

$$\rho_f A_p C_P\frac{\partial T_f}{\partial t}+\rho_f A_p C_P u\cdot\nabla T_f=\nabla\cdot(\lambda_f A_P\nabla T_f)+\frac{1}{2}f_D\frac{\rho A_p}{2d_h}|u|u^2+Q+Q_{wall} \tag{3}$$

where ρ_f is the fluid density ($kg\,m^{-3}$), A_p is the pipe cross section area (m^2), C_p represents the specific heat capacity at a constant pressure ($J\,kg^{-1}\,K^{-1}$), u is the tangential velocity of the fluid ($m\,s^{-1}$), T_f is the fluid temperature (K), and λ_f is the fluid thermal conductivity ($W\,m^{-1}\,K^{-1}$). Furthermore, $\frac{1}{2}f_D\frac{\rho A_p}{2d_h}|u|u^2$ indicates the friction heat dissipated due to viscosity, for which Churchill's friction model was used to calculate the coefficient of friction (f_D) [27], and d_h is the mean hydraulic diameter (m). Q represents a general heat source, and Q_{wall} denotes the heat source term that results from heat exchange with the surroundings through the pipe wall. The equation between the pipe flow and heat conduction of the solid mass can be coupled through the following term (Eq. (4)). This process is also schematized in Fig. 2.

$$Q_{wall}=(hZ)_{eff}(T_{ext}-T_f)\ (W/m) \tag{4}$$

where T_{ext} is the external temperature outside the pipe (K), and $(hZ)_{eff}$ is the effective hZ, which corresponds to an equivalent convective heat transfer coefficient, i.e. h (SI unit: $W\,m^{-2}\,K^{-1}$) × the wall perimeter Z (SI unit: m), of the pipe. For a circular tube, the effective hZ can be denoted as follows:

$$(hZ)_{eff}=\frac{2\pi}{\frac{1}{r_0 h_{int}}+\frac{1}{r_N h_{ext}}+\sum_{n=1}^{N}\left(\frac{\ln\frac{r_n}{r_{n-1}}}{\lambda_n}\right)} \tag{5}$$

where λ_n is the thermal conductivity (W/m K) of wall n, r_n (m) is the outer radius of wall n, and h_{int} and h_{ext} are the film heat transfer coefficients inside and outside the tube ($W\,m^{-2}\,K^{-1}$), respectively.

4. Economic analysis theory

When evaluating the validity of an investment business, an economic analysis is essential. An economic analysis evaluates whether the business overall will experience an increase or a decrease in net benefits. There are several economic analysis methods that can consider the economic benefits for each particular business.

Net present value (NPV) is defined as the sum of the present values (PVs) of incoming and outgoing cash flows over a period of time. Here, incoming and outgoing cash flows can also be described as benefit and cost cash flows, respectively. Following is the formula for calculating NPV:

$$\mathrm{NPV}=\sum_{n=1}^{N}\frac{R_n}{(1+r)^n}-P_0 \tag{6}$$

where R_n is the net cash inflow in the period $n=1$ to N, and this study assumed that the total period is 10 years ($N=10$). P_0 is the initial investment in period zero (a positive number shown with a minus sign to indicate that money is paid away), r is the discount rate and n is the number of time periods. The internal rate of return (IRR) means the value of the discount rate (r) where the NPV is 0. In general, the higher a project's internal rate of return, the more desirable it is to undertake the project. Therefore, IRR can be used to rank several prospective projects that a firm is considering. Assuming all other factors are equal among the various projects,

Table 5
A total of 160 parameter combinations used in parametric studies.

Case	Pitch (m)	Setting depth (m)	Fluid velocity ($m\,s^{-1}$)	Case	Pitch (m)	Setting depth (m)	Fluid velocity ($m\,s^{-1}$)	Case	Pitch (m)	Setting depth (m)	Fluid velocity ($m\,s^{-1}$)
1	0.02	1	0.5	61	0.08	1	0.5	121	0.20	1	0.5
2	0.02	1	0.7	62	0.08	1	0.7	122	0.20	1	0.7
3	0.02	1	0.9	63	0.08	1	0.9	123	0.20	1	0.9
4	0.02	1	1.1	64	0.08	1	1.1	124	0.20	1	1.1
5	0.02	1	1.3	65	0.08	1	1.3	125	0.20	1	1.3
6	0.02	1.5	0.5	66	0.08	1.5	0.5	126	0.20	1.5	0.5
7	0.02	1.5	0.7	67	0.08	1.5	0.7	127	0.20	1.5	0.7
8	0.02	1.5	0.9	68	0.08	1.5	0.9	128	0.20	1.5	0.9
9	0.02	1.5	1.1	69	0.08	1.5	1.1	129	0.20	1.5	1.1
10	0.02	1.5	1.3	70	0.08	1.5	1.3	130	0.20	1.5	1.3
11	0.02	2	0.5	71	0.08	2	0.5	131	0.20	2	0.5
12	0.02	2	0.7	72	0.08	2	0.7	132	0.20	2	0.7
13	0.02	2	0.9	73	0.08	2	0.9	133	0.20	2	0.9
14	0.02	2	1.1	74	0.08	2	1.1	134	0.20	2	1.1
15	0.02	2	1.3	75	0.08	2	1.3	135	0.20	2	1.3
16	0.02	2.5	0.5	76	0.08	2.5	0.5	136	0.20	2.5	0.5
17	0.02	2.5	0.7	77	0.08	2.5	0.7	137	0.20	2.5	0.7
18	0.02	2.5	0.9	78	0.08	2.5	0.9	138	0.20	2.5	0.9
19	0.02	2.5	1.1	79	0.08	2.5	1.1	139	0.20	2.5	1.1
20	0.02	2.5	1.3	80	0.08	2.5	1.3	140	0.20	2.5	1.3
21	0.03	1	0.5	81	0.10	1	0.5	141	0.25	1	0.5
22	0.03	1	0.7	82	0.10	1	0.7	142	0.25	1	0.7
23	0.03	1	0.9	83	0.10	1	0.9	143	0.25	1	0.9
24	0.03	1	1.1	84	0.10	1	1.1	144	0.25	1	1.1
25	0.03	1	1.3	85	0.10	1	1.3	145	0.25	1	1.3
26	0.03	1.5	0.5	86	0.10	1.5	0.5	146	0.25	1.5	0.5
27	0.03	1.5	0.7	87	0.10	1.5	0.7	147	0.25	1.5	0.7
28	0.03	1.5	0.9	88	0.10	1.5	0.9	148	0.25	1.5	0.9
29	0.03	1.5	1.1	89	0.10	1.5	1.1	149	0.25	1.5	1.1
30	0.03	1.5	1.3	90	0.10	1.5	1.3	150	0.25	1.5	1.3
31	0.03	2	0.5	91	0.10	2	0.5	151	0.25	2	0.5
32	0.03	2	0.7	92	0.10	2	0.7	152	0.25	2	0.7
33	0.03	2	0.9	93	0.10	2	0.9	153	0.25	2	0.9
34	0.03	2	1.1	94	0.10	2	1.1	154	0.25	2	1.1
35	0.03	2	1.3	95	0.10	2	1.3	155	0.25	2	1.3
36	0.03	2.5	0.5	96	0.10	2.5	0.5	156	0.25	2.5	0.5
37	0.03	2.5	0.7	97	0.10	2.5	0.7	157	0.25	2.5	0.7
38	0.03	2.5	0.9	98	0.10	2.5	0.9	158	0.25	2.5	0.9
39	0.03	2.5	1.1	99	0.10	2.5	1.1	159	0.25	2.5	1.1
40	0.03	2.5	1.3	100	0.10	2.5	1.3	160	0.25	2.5	1.3
41	0.05	1	0.5	101	0.15	1	0.5				
42	0.05	1	0.7	102	0.15	1	0.7				
43	0.05	1	0.9	103	0.15	1	0.9				
44	0.05	1	1.1	104	0.15	1	1.1				
45	0.05	1	1.3	105	0.15	1	1.3				
46	0.05	1.5	0.5	106	0.15	1.5	0.5				
47	0.05	1.5	0.7	107	0.15	1.5	0.7				
48	0.05	1.5	0.9	108	0.15	1.5	0.9				
49	0.05	1.5	1.1	109	0.15	1.5	1.1				
50	0.05	1.5	1.3	110	0.15	1.5	1.3				
51	0.05	2	0.5	111	0.15	2	0.5				
52	0.05	2	0.7	112	0.15	2	0.7				
53	0.05	2	0.9	113	0.15	2	0.9				
54	0.05	2	1.1	114	0.15	2	1.1				
55	0.05	2	1.3	115	0.15	2	1.3				
56	0.05	2.5	0.5	116	0.15	2.5	0.5				
57	0.05	2.5	0.7	117	0.15	2.5	0.7				
58	0.05	2.5	0.9	118	0.15	2.5	0.9				
59	0.05	2.5	1.1	119	0.15	2.5	1.1				
60	0.05	2.5	1.3	120	0.15	2.5	1.3				

the project with the highest IRR would probably be considered the best and undertaken first. However, often, the value of r cannot be obtained analytically. In this case, numerical methods should be used. There are several numerical methods that can be used to estimate r. For example, using the secant method [28], the internal rate of return (IRR) can be calculated as indicated in Eq. (7).

$$r_{n+1} = r_n - \mathrm{NPV}_n\left(\frac{r_n - r_{n-1}}{\mathrm{NPV}_n - \mathrm{NPV}_{n-1}}\right) \tag{7}$$

where r_n is considered the nth approximation of the IRR. In this study, the IRR calculation algorithm was suggested using the secant method (Fig. 3). The algorithm is implemented via MATLAB code, and hence the IRR value can be obtained automatically after several iterative calculations as shown in Fig. 4.

Savings to investment ratio (SIR) is a dimensionless measure of performance that expresses the ratio of savings to cost for a specific period. In this study, the period was assumed to be 10 years. The numerator of the ratio contains the operation-related savings; the

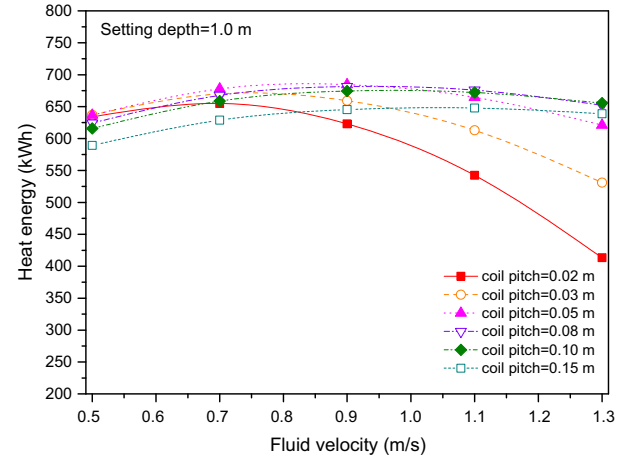

(a) Setting depth = 1.0 m

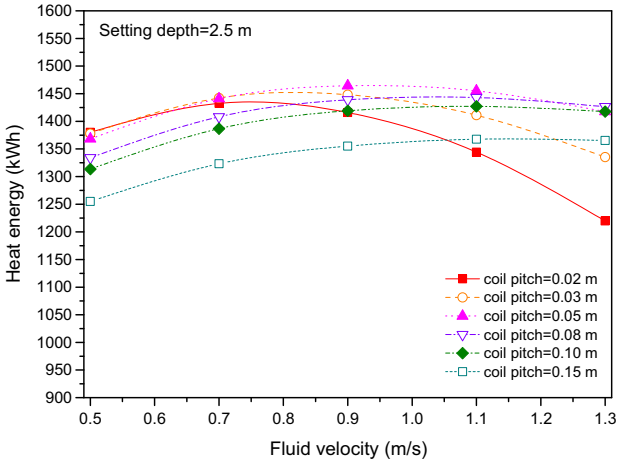

(b) Setting depth = 2.5 m

Fig. 10. Parametric study results for heat energy of horizontal ground coupled heat pumps.

denominator contains the increase in investment-related costs. SIR is used for establishing priorities among projects. Within the specified time frame: values of '1' indicate that the investment cost was completely recouped; values >1 indicate savings greater than the investment, values <1 indicate the investment cost was more than the potential savings from the system.

The simple payback period (SPP) is the number of years required to recover the initial investment through the projected savings. This is a good first cut investment analysis tool, but it does not take into account the time value of money. In this study, we have taken the total project cost, and divided that amount by the annual savings. After calculating the SPP for each alternative, the alternative with the shortest payback period is regarded as the optimal choice.

5. Results and discussion

5.1. Indoor thermal response test

Fig. 5 shows the fluid temperature variations for differences in coil pitch during the indoor thermal response tests. Inlet and outlet fluid temperatures increased nonlinearly as the time elapsed, but the difference between inlet and outlet temperatures appeared to be converging to a constant value. Because a constant flow rate was injected during each test (Table 2), the heat injection (Q) was also converging to a certain value. The average heat injection (Q) of each test (Test I–Test IV) was 430 W, 385 W, 374 W, and 296 W, respectively. In this study, a 3D finite element model was developed to simulate the indoor thermal response tests. As can be seen in Fig. 6, the prediction of the numerical simulation model was in good agreement with the results of the indoor thermal response tests for both fluid temperature and soil medium temperature. According to the results of error analysis of the measurement (Fig. 7), the average relative error showed less than 2.5% except one case. A little disagreement occurred for the prediction of ground temperature at Point A in Test II (average relative error is 3.92%, maximum relative error is 8.85%), it is thought that the misplacement of the RTD sensor would have caused this disagreement.

5.2. Parametric study

Once the reliability of the numerical simulation model has been evaluated with experimental data, the numerical simulation model provides a convenient way of conducting parametric studies. Since good agreements in prediction were observed during the thermal response test, it can be considered that the numerical simulation model is suitable for predicting the heat transfer behavior of hori-

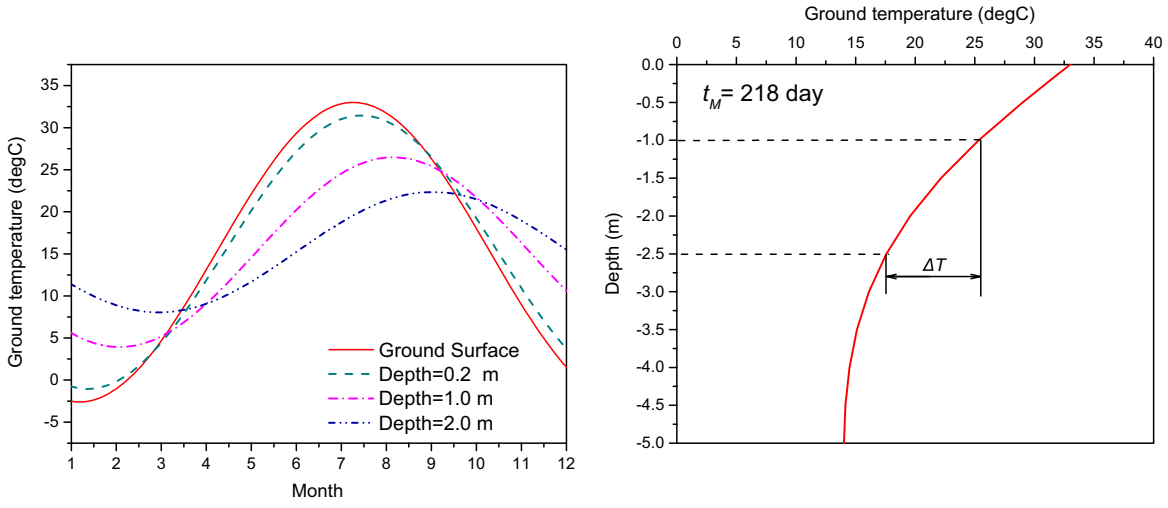

Fig. 11. Ground temperature variation according to ground depth.

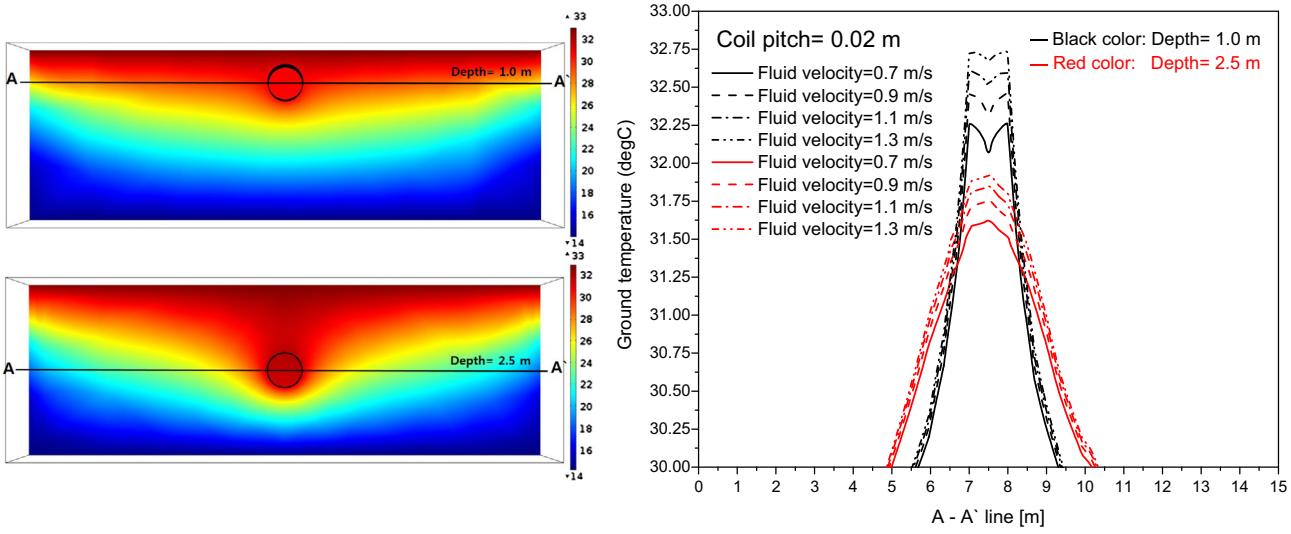

Fig. 12. Ground temperature variation around heat exchanger at steady state.

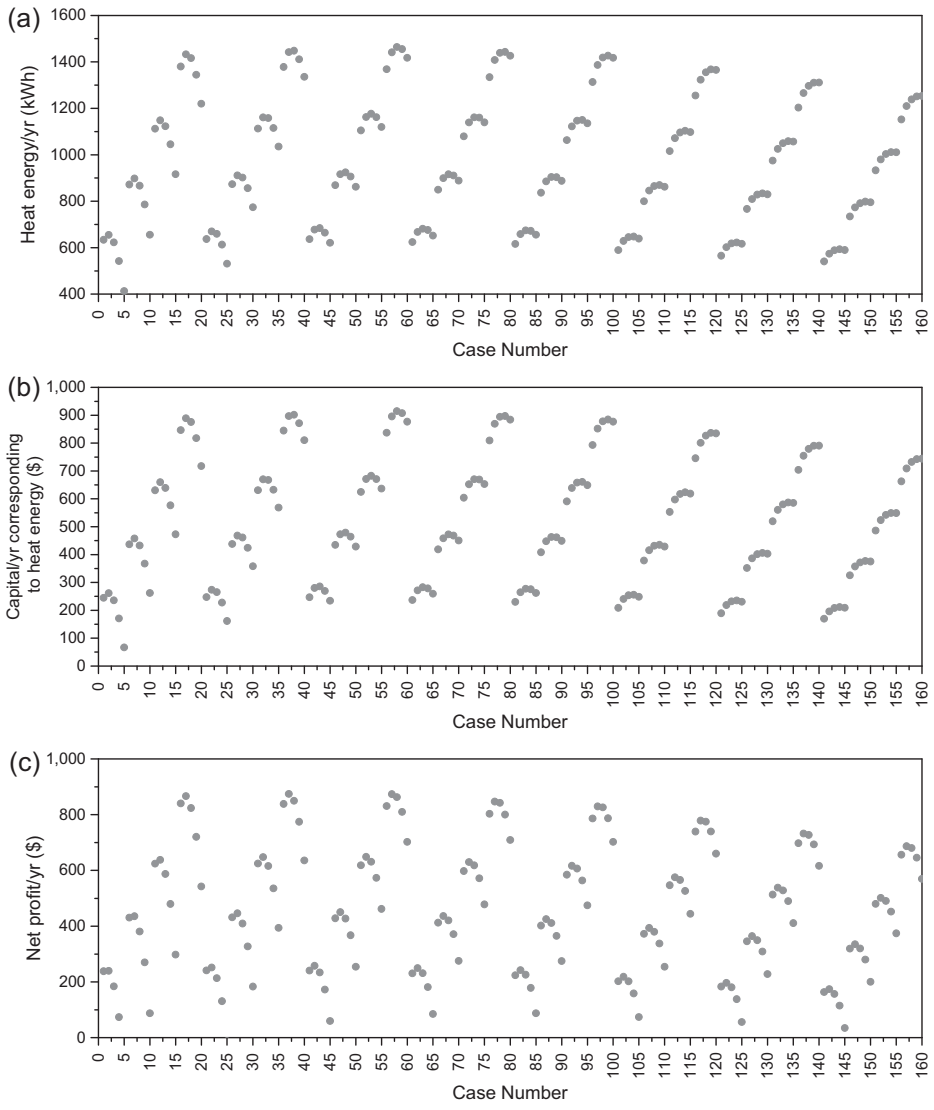

Fig. 13. Comparison of results by design conditions: (a) Heat energy/yr; (b) capital/yr corresponding to heat energy, (c) net profit/year.

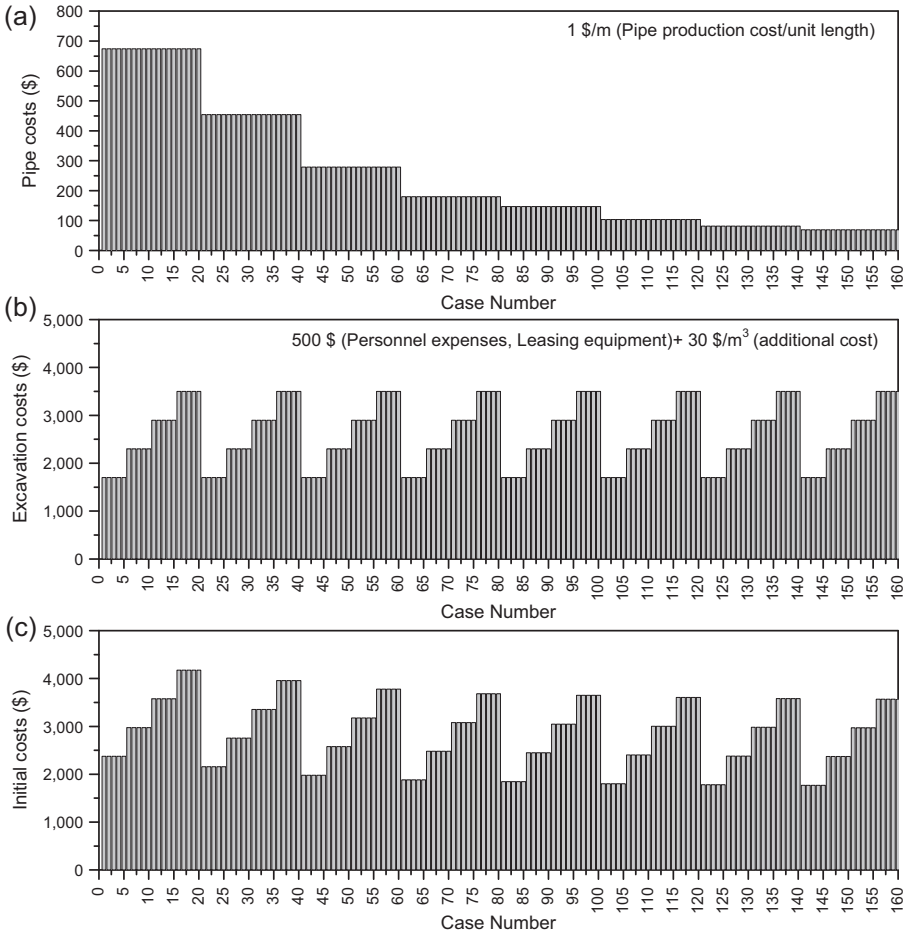

Fig. 14. Comparison of installation costs: (a) Pipe cost, (b) excavation cost, (c) initial cost.

Table 6
A standard electricity charge per kW h (for residential building).

Basic charge ($/house)		Energy charge ($/kW h)	
Using less than 100 kWh	0.410	0–100 kW h	0.0607
Using 101–200 kW h	0.910	101–200 kW h	0.1259
Using 201–300 kW h	1.600	201–300 kW h	0.1879
Using 301–400 kW h	3.850	301–400 kW h	0.2806
Using 401–500 kW h	7.300	401–500 kW h	0.4177
Using more than 501 kW h	12.940	More than 501 kW h	0.7095

Provided by KEPCO (Korea Electric Power Corporation).

zontal GCHPs. Thus, the numerical simulation models were used to conduct parametric studies in this study, to grasp the degree of effects of input parameters used in the model, on the output. These results were ultimately used to propose an optimum design of horizontal GCHPs. For the parametric studies, a finite element model was developed with dimensions of 30 m × 15 m × 5 m (width × height × depth), as shown in Fig. 8. Polybutylene spiral-coil heat exchangers (λ = 0.39 W m^{-1} K^{-1}) were modeled, of which the coil diameter, outer pipe diameter, and thickness were 0.50 m, 0.025 m, and 0.002 m, respectively. The length of the axial return pipe was 16.0 m. The spiral-coil-type pipeline, which exhibits a steep temperature gradient, was modeled using extremely fine mesh for accurate calculations. However, the surrounding domain was modeled using coarser meshes to reduce memory size and calculation time. Fig. 9 presents the grid independence test results. According to the test results, the outlet temperature tended to converge toward a constant value when the number of elements exceeded about 90,000. Hence, the domain consisted of free tetrahedral meshes with maximum element size of 2.4 m and minimum size of 0.30 m (a total of 103,148 elements).

Table 7
Comparison of pump operating costs according to fluid velocity.

Fluid velocity (m s^{-1})	LPM	Power consumption (kW h)	Cost ($/kW h)
0.5	6.032	82.59	6.190
0.7	8.445	198.57	22.090
0.9	10.857	314.55	51.740
1.1	13.270	430.53	97.020
1.3	15.683	546.51	174.600

Table 8
Initial installation costs.

Pipe production cost	$1/m
Personnel expenses, leasing equipment	500 $
Trench excavation/backfill cost	$30/m^3

The material properties used in the numerical model are presented in Table 3, and it was supposed that the ground properties were constant at all depths and temperatures [29]. In order to model the temperature profile in the ground as a function of the depth (z) and time (t), Eq. (8) was used [29,30] to set the boundary conditions (Fig. 8).

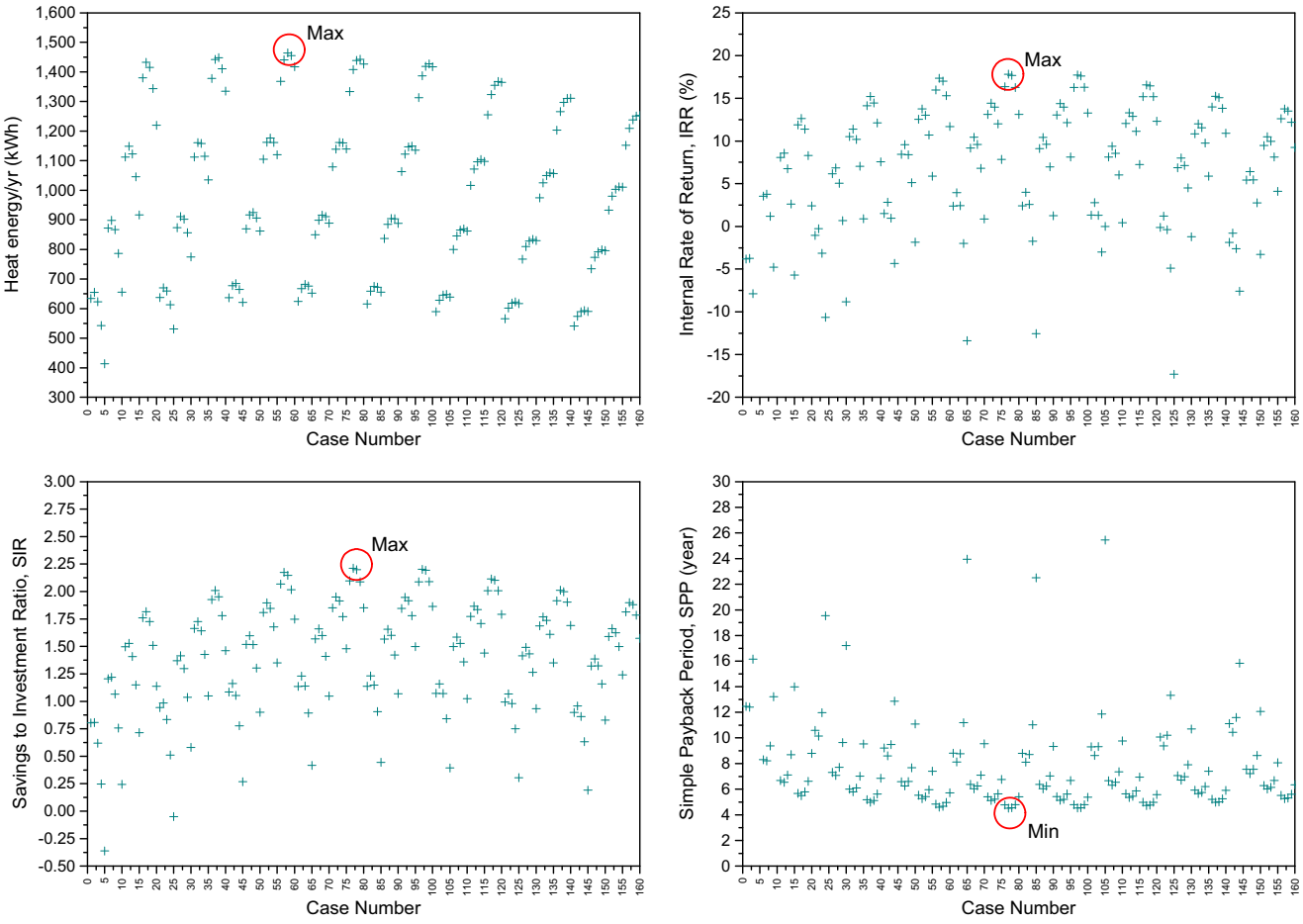

Fig. 15. Comparison of alternatives through economic analysis.

Table 9
Summary of maximum values from the parametric studies and economic analyses.

Index	Value	Case number	Coil pitch (m)	Setting depth (m)	Fluid velocity ($m\,s^{-1}$)
Heat energy/yr_max (kWh)	1464.43	58	0.05	2.5	0.9
IRR_max (%)	17.83	77	0.08	2.5	0.7
SIR_max	2.21	77	0.08	2.5	0.7
SPP_min (yr)	4.52	77	0.08	2.5	0.7

$$T(z,t) = T_M + a \cdot e^{-z\sqrt{\frac{\omega}{2D_T}}} \sin\left(\omega t - z\sqrt{\frac{\omega}{2D_T}} + b\right)$$
$$\omega = 2\pi/\tau \qquad (8)$$
$$b = (\tau - 4t_M)\pi/2\tau$$

where T_M is the mean temperature in the year of the climatic zone; a is the half difference between the maximum and minimum annual temperatures on the soil surface; τ is the considered period; t_M is the time when the maximum temperature on the ground surface occurs; and D_T is the thermal diffusivity of the considered soil. The values of the constants used in Eq. (8) are those presented in Table 4. Furthermore, the temperature boundary condition of the inlet pipeline was set at the ground surface temperature, and the performance was evaluated in cooling mode. As for hydraulic boundary condition, the flow rate at inlet pipe was set at one of five different levels (0.5, 0.7, 0.9, 1.1, or 1.3 $m\,s^{-1}$). Also, the hydraulic gradient in the ground was assumed to be zero; it means that groundwater advection was not considered. The HGCHPs were supposed to operate only when the connected heat pump was switched on: the activation days and hours were from 1 June to 31 August, every day from 8:00 am to 7:00 pm.

Meanwhile, the parametric studies were conducted by analyzing the trend of heat performance for the change of input parameter value within a possible range. The input parameters affecting the optimum design of the GCHP were as follows: coil pitch, installation depth, and fluid velocity. Table 5 presents the 160 parameter combinations used in the parametric studies. Various heat exchangers with coil pitches of 0.02, 0.03, 0.05, 0.08, 0.10, 0.15, 0.20, and 0.25 m were considered. The flow rate of the circulating fluid was set at one of five different levels (0.5, 0.7, 0.9, 1.1, or 1.3 $m\,s^{-1}$) in order to verify the influence of inlet fluid velocity on the heat transfer capabilities of each configuration. Furthermore, four different setting depths (1.0, 1.5, 2.0 and 2.5 m) were considered in order to examine the effect of ground surface temperature on system performance.

Fig. 10 shows the results of the parametric studies for optimum design of spiral coil HGCHPs. Overall, it was ascertained that the heat efficiency was much higher when the installation depth was 2.5 m compared with the case when the installation depth was 1.0 m. As shown in Fig. 11, the ground temperature difference between depth 1.0 m and depth 2.5 m was more than 7.5 °C (t_M = 218 day). Because the heat efficiency of HGCHPs is significantly affected by the ground temperature (the heat exchange medium), the heat efficiency of the system was more than doubled at the greater depth.

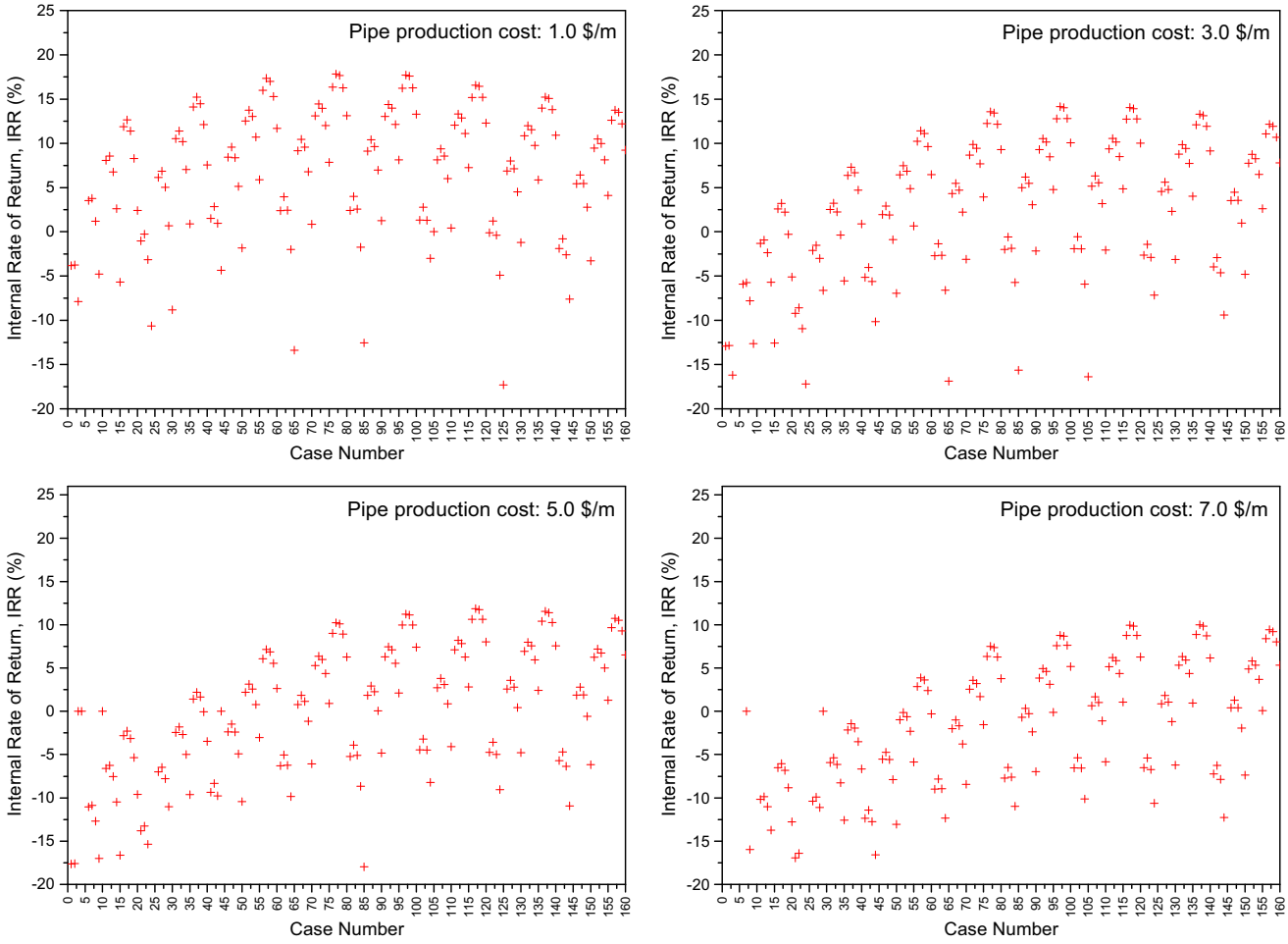

Fig. 16. Variation of IRR with increase of pipe production cost.

Moreover, as the coil pitch became narrower, the area of thermal diffusion increased; hence, the total amount of heat exchange also tended to increase. However, if the coil-pitch was too narrow, the heat efficiency decreased due to thermal interference among the pipes. This becomes more serious when the inlet fluid velocity is high. Fig. 12 shows the ground temperature distribution around the heat exchanger for a narrow coil pitch (pitch = 0.02 m). As the fluid velocity increased from 0.7 m s^{-1} to 1.3 m s^{-1}, the ground temperature near the heat exchanger rapidly increased. In general, an increase of the flow rate has a positive influence on the performance of the heat exchanger, but if the coil pitch becomes too narrow, total efficiency will decrease in inverse proportion to flow rate. In this case, the difference in fluid temperature between the inlet and outlet rapidly decreases due to thermal interference. Especially, when the ground heat exchanger was installed at a shallow depth (1.0 m), the ground temperature near the heat exchanger increased to 32.75 °C, and the system's heat efficiency decreased further.

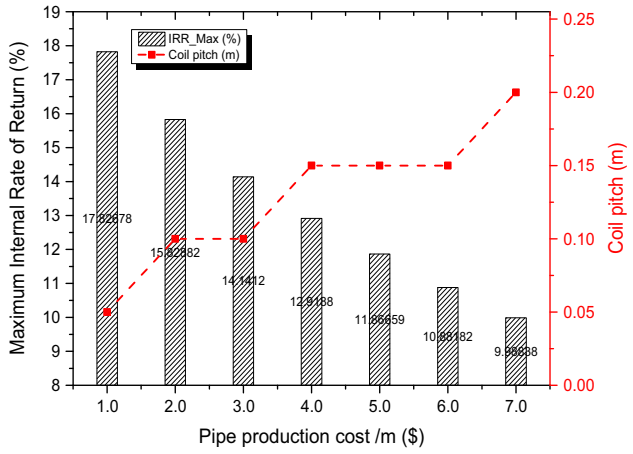

Fig. 17. Maximum IRR in relation to pipe production cost and optimal design conditions.

5.3. Optimum design of HGCHPs

Fig. 13 shows the comprehensive results of the parametric studies detailed in Table 5. Through the developed numerical simulation model, the heat energy and the capital values were compared with each other according to a total of 160 major design-factor combinations. When considering only efficiency aspects, the maxima were: annual heat energy 1464.3 kW h; coil pitch 0.05 m, setting depth 2.5 m, and fluid velocity 0.9 m s^{-1} (Case 58). Supposing that the GCHP provides all the cooling energy loads, the annual heat energy can be converted into annual capital. Table 6 shows the unit price of electricity charge per kWh considering basic rate and progressive tax. Using this table, the capital values can be represented according to design factor combinations (Fig. 13b). Meanwhile, differences in operational costs occur because the pump's circulation power changes with the flow rate.

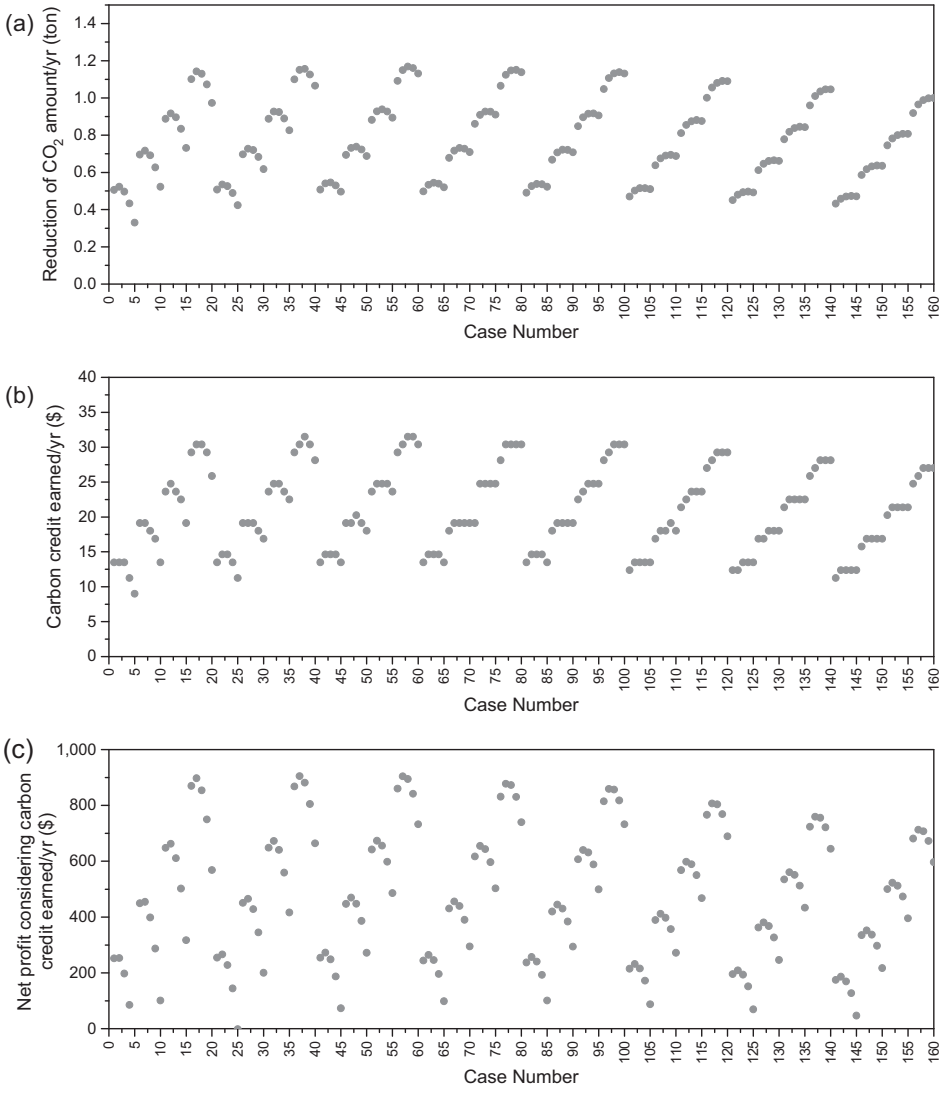

Fig. 18. Impact of carbon credit earned: (a) Reduction of CO_2 amount/year; (b) carbon credit earned/year; (c) net profit considering carbon credit earned/year.

Based on the operational cost per kW h by flow rate, as presented in Table 7, the annual net profit can be derived from the operational cost reflected in the energy acquisition cost. As shown in Fig. 13(c), when comparing the annual net profit considering pump operation costs, the maximum annual net profit was $874.74, coil pitch was 0.03 m, setting depth was 2.5 m, and fluid velocity was 0.7 m s^{-1} (case 37). These results show that the design parameters should be estimated after considering the pump operation costs.

Another factor to be considered for optimal design of HGCHPs is the cost of the initial investment. Instead of focusing only on system efficiency in the design stage, more realistic and economical alternatives can be developed by taking into account the efficiency in relation to the investment cost. The initial investment costs include pipe production costs and excavation costs. The excavation costs include those for leasing equipment, personnel expenses, and additional costs according to the scale of excavation. As can be seen in Fig. 14, this study indicated the initial investment costs for each case, based on the assumptions in Table 8.

Fig. 15 shows the results of economic analysis for each design condition considering the annual net profits and initial investment costs. As indicated in Table 9, when considering only aspects of system efficiency, Case 58 (design conditions: coil pitch 0.05 m, setting depth 2.5 m, and fluid velocity 0.9 m s^{-1}) was the best case, but the economic analysis factors such as Internal Rate of Return (IRR), Savings to Investment Ratio (SIR), Simple Payback Period (SPP) showed that Case 77 (design conditions: coil pitch 0.08 m, setting depth 2.5 m, and fluid velocity 0.7 m s^{-1}) had the most economic feasibility. Thermal efficiency improves as the coil pitch grows narrower, but the optimal design size of a coil pitch increases from 0.05 m to 0.08 m because the former involves higher pipe costs. In addition, considering the thermal interference between pipes and the operational cost of the pump, optimal flow rate conditions were observed at 0.7 m/s. The optimal installation depth was found to be 2.5 m in all three analyses of economic efficiency, implying that a greater depth is preferred despite the higher digging cost. Consequently, it can be inferred that the enhanced thermal efficiency of the system at greater depth is sufficient to compensate for the higher cost required for digging.

However, because the pipe production cost changes with country and manufacturer, the economic feasibility of each design factor combination may vary with the unit cost of pipe production. Fig. 16 indicates that the IRR varies with the unit cost of pipe production for all the design combinations. As the production cost increases, the IRR tends to decrease. Furthermore, the design condition that maximizes the IRR also varies, Fig. 17 shows the maximum IRR in relation to pipe production cost and the corresponding

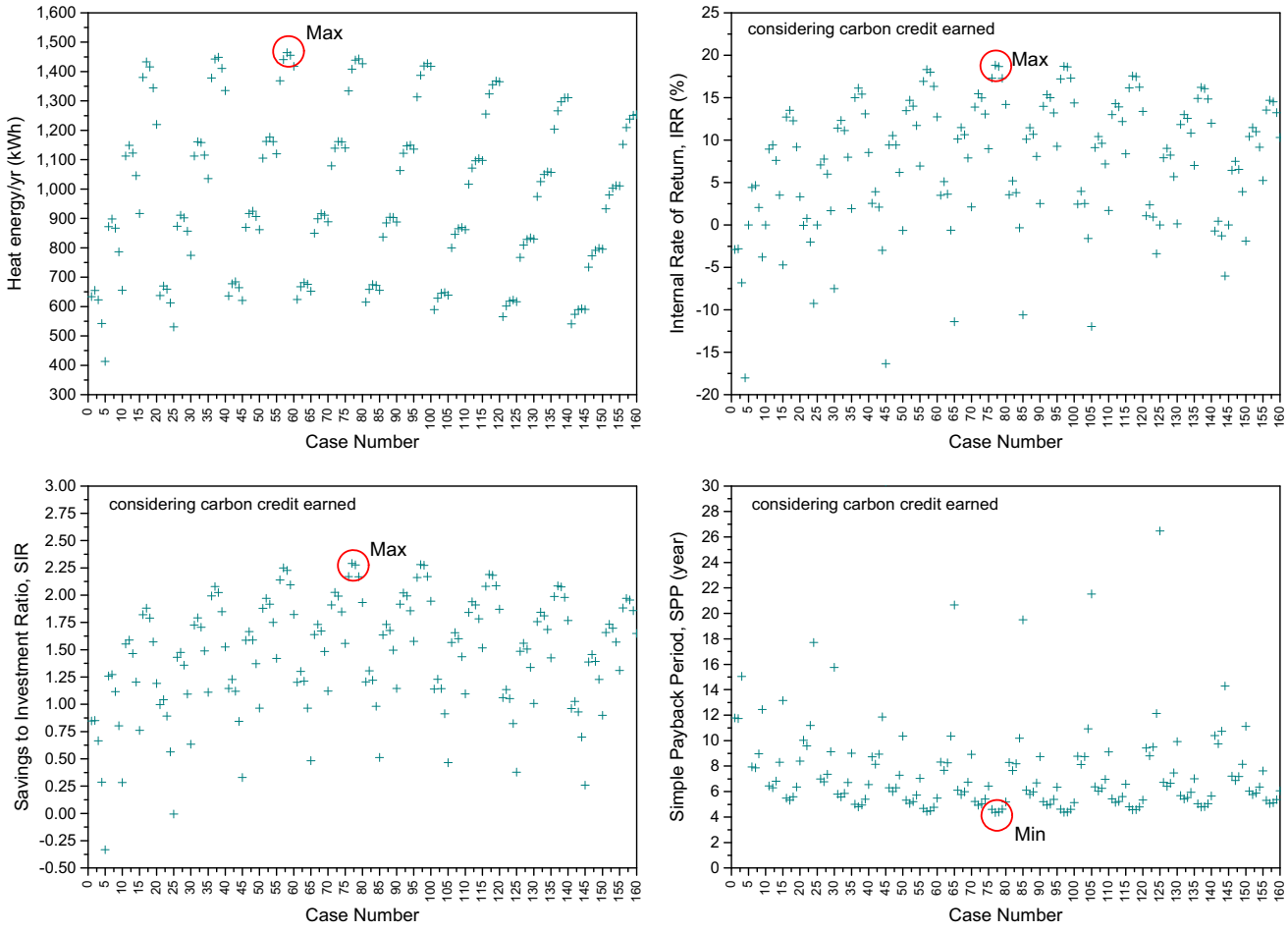

Fig. 19. Comparison of alternatives considering carbon credit earned through economic analysis.

optimal design conditions. When the unit cost of pipe production increased from $1 to $7, the IRR decreased by 35%, and the optimum design size of a coil pitch increased from 5 cm to 20 cm. Thus, it can be confirmed that the optimum design condition will be sensitive to the estimation standard of the initial investment costs in the design phase.

Along with the cost of the initial investment, the environmental benefits of the system can also be considered in design phase. Fig. 18(a) shows the reduction amount of CO_2 emission of HGCHPs for each design condition compared to a typical HVAC system. When the HVAC system is substituted to a proposed HGCHPs, the CO_2 emission amount can be reduced by up to 1.169 ton per year. This can earn the carbon credits and simultaneously cause a great advantage in annual net profit, as shown in Fig. 18(b) and (c). Fig. 19 shows the impact of carbon credits earned on internal rate of return (IRR), net present value (NPV) and payback period (PBP). When considering carbon credits earned, the IRR and SIR increased 5.6%, and 3.7%, respectively, and payback period decreased 0.15 year in optimum design condition.

6. Conclusions and summary

In this study, we proposed an optimum design for a horizontal ground-coupled heat pump system (HGCHP) for spiral-coil-loop heat exchanger. A 3D numerical analysis model simulating the thermal behavior of a spiral coil HGHE was developed, and the accuracy of the model was verified using indoor thermal response tests (TRTs). After that, a total of 160 parametric studies were conducted using the numerical simulation models in order to determine the degree of effect that the input parameters used in the model would have on the output. From this, an optimum design condition was proposed for horizontal GCHPs using several economic analysis tools that could consider the economic benefits of each particular design condition. The main conclusions drawn from the study results can be summarized as follows:

1. The thermal response tests (TRTs) of spiral coil HGHE were conducted in a model chamber. Also, a 3D finite element model was developed to simulate the indoor thermal response tests. Because the prediction of the numerical simulation model was in good agreement with the results of the indoor thermal response tests, the developed numerical simulation model was able to provide a basis for conducting the parametric studies.
2. As the coil pitch becomes narrow, the area of thermal diffusion increases; hence, the total amount of heat exchange also tends to increase. However, if the coil pitch is extremely narrow, the heat efficiency decreases due to thermal interference among the pipes. This becomes more extreme when inlet fluid velocity is fast.
3. Through the newly developed numerical simulation model, the heat efficiencies were compared for 160 major combinations of design factors. When considering only efficiency, the maxima were annual heat energy 1464.3 kW h; coil pitch 5 cm, setting depth 2.5 m, and fluid velocity 0.9.
4. However, if the cost of initial investment is considered, the optimal design size of a coil pitch increases from 5 cm to 8 cm because the former involves higher pipe costs. In addition, con-

sidering the thermal interference between pipes and the operational cost of the pump, optimal flow rate conditions are observed at 0.7 m/s. The optimal installation depth appears to be 2.5 m (in all the economic analyses), implying that a greater depth is preferred despite the higher digging cost. Therefore, it can be inferred that the enhanced thermal efficiency of the system at greater depth is sufficient to compensate for the higher cost for additional digging.

5. The pipe production cost changes with country and manufacturer, and then the economic feasibility of each design factor combination may vary with the unit cost of pipe production. When the unit cost of pipe production increases, the IRR will decrease, the optimum design size of a coil pitch will increase. With these results, it can be inferred that the optimum design condition is sensitive to variations in the estimation standard of initial investment costs in the design phase.
6. Along with the cost of the initial investment, the environmental benefits of the system can also be considered in design phase. When the HVAC system is substituted to a proposed HGCHPs, the CO_2 emission amount can be reduced by up to 1.169 ton per year. This can earn the carbon credits and simultaneously cause a great advantage in annual net profit. When considering carbon credits earned, the IRR and SIR increased 5.6%, and 3.7%, respectively, and payback period decreased 0.15 year in optimum design condition.

Acknowledgements

This work was financially supported by Korea Minister of Ministry of Land, Infrastructure and Transport (MOLIT) as U-City Master and Doctor Course Grant Program and by grant 15RDRP-B076564-02 from the Regional Development Research Program funded by the Ministry of Land, Infrastructure and Transport of the Korean government.

References

[1] Omer AM. Ground-source heat pumps systems and applications. Renew Sust Energy Rev 2008;12:344–71.
[2] Chua KJ, Chou SK, Yang WM. Advances in heat pump systems: a review. Appl Energy 2010;87:3611–24.
[3] Li M, Lai ACK. New temperature response functions (G functions) for pile and borehole ground heat exchangers based on composite-medium line-source theory. Energy 2012;38:255–63.
[4] Zarrella A, Carli MD, Galgaro A. Thermal performance of two types of energy foundation pile: helical pipe and triple U-tube. Appl Therm Eng 2013;61:301–10.
[5] Edwards KC, Finn DP. Generalised water flow rate control strategy for optimal part load operation of ground source heat pump systems. Appl Energy 2015;150:50–60.
[6] Congedo PM, Colangelo G, Starace G. CFD simulation of horizontal ground heat exchangers: a comparison among different configurations. Appl Therm Eng 2012;33–34:24–32.
[7] Tarnawski VR, Leong WH, Momose T, Hamada Y. Analysis of ground source heat pumps with horizontal ground heat exchangers for northern Japan. Renew Energy 2009;34:127–34.
[8] Wu Y, Gan G, Verhoef A, Vidale PL, Gonzalez RG. Experimental measurement and numerical simulation of horizontal-coupled slinky ground source heat exchangers. Appl Therm Eng 2010;30(16):2574–83.
[9] Sanaye S, Niroomand B. Horizontal ground coupled heat pump: thermal-economic modeling and optimization. Energy Convers Manage 2010;51:2600–12.
[10] Li H, Nagano K, Lai Y. Heat transfer of a horizontal spiral heat exchanger under groundwater advection. Int J Heat Mass Trans 2012;55(23–24):6819–31.
[11] Gonzalez RG, Verhoef A, Vidale PL, Main B, Gan G, Wu Y. Interactions between the physical soil environment and a horizontal ground coupled heat pump, for a domestic site in the UK. Renew Energy 2012;44:141–53.
[12] Fujii H, Yamasaki S, Maehara T, Ishikami T, Chouc N. Numerical simulation and sensitivity study of double-layer slinky-coil horizontal ground heat exchangers. Geothermics 2013;47:61–8.
[13] Chong CSA, Gan G, Verhoef A, Garcia RG, Vidale PL. Simulation of thermal performance of horizontal slinky-loop heat exchangers for ground source heat pumps. Appl Energy 2013;104:603–10.
[14] Bazkiaei AR, Niri ED, Kolahdouz EM, Weber AS, Dargush GF. A passive design strategy for a horizontal ground source heat pump pipe operation optimization with a non-homogeneous soil profile. Energy Build 2013;61:39–50.
[15] Go GH, Lee SR, Nikhil NV, Yoon S. A new performance evaluation algorithm for horizontal GCHPs (ground coupled heat pump systems) that considers rainfall infiltration. Energy 2015;83:766–77.
[16] Adamovsky D, Neuberger P, Adamovsky R. Changes in energy and temperature in the ground mass with horizontal heat exchangers—the energy source for heat pumps. Energy Build 2015;92:107–15.
[17] Kupiec K, Larwa B, Gwadera M. Heat transfer in horizontal ground heat exchangers. Appl Therm Eng 2015;75:270–6.
[18] Naylor S, Ellett KM, Gustin AR. Spatiotemporal variability of ground thermal properties in glacial sediments and implications for horizontal ground heat exchanger design. Renew Energy 2015;81:21–30.
[19] Netzsch. Heat flow meters HFM 436 Lambda series. Netzsch, Selb, Germany; 2013.
[20] Hukseflux. User manual of TP08: small size non-steady probe for thermal conductivity measurement. Delft, Netherlands: Hukseflux Thermal Sensors; 2006.
[21] Comsol Inc. Comsol multiphysics user's manual Ver. 5.0a. USA; 2014.
[22] Bear J, Bachmat Y. Introduction to modeling of transport phenomena in porous media. Kluwer Academic Publisher; 1990.
[23] Moyne C, Didierjean S, Amaral Souto HP, da Silveira OT. Thermal dispersion in porous media: one-equation model. Int J Heat Mass Transfer 2000;43(20):3853–67.
[24] Nield DA, Bejan A. Convection in porous media, in convection heat transfer. 4th ed. Hoboken, NJ, USA: John Wiley & Sons Inc.; 2013.
[25] Incropera FP, DeWitt DP. Fundamentals of heat and mass transfer. 6th ed. John Wiley & Sons; 2005.
[26] Lurie MV. Modeling of oil product and gas pipeline transportation. Weinheim: WILEY-VCH Verlag GmbH & Co., KGaA; 2008.
[27] Churchill SW. Friction factor equations span all fluid-flow regimes. Chem Eng 1997;84(24):91.
[28] Kaw AK, Kalu EE, Nguyen D. Numerical methods with applications. 2nd ed. University of South Florida; 2009.
[29] Cavazza L. Fisica del terreno agrario. Torino, Italy: UTET; 1981.
[30] Kirkham D, Powers WL. Advanced soil physics. New York, USA: J. Wiley-Interscience; 1972.